RSC Advances

PAPER

View Article Online
View Journal | View Issue

Cite this: *RSC Adv.*, 2023, **13**, 5186

Preparation of core–shell catalyst for the tandem reaction of amino compounds with aldehydes†

Jinhua Liang, [a] Lan Wu,*[a] Zhenhua Li, *[a] Yang Liu,[a] Nana Ding[a] and Zhengping Dong *[b]

Heterogeneous noble metal-based catalysts with stable, precise structures and high catalytic performance are of great research interest for sustainable catalysis. In this article, we designed a novel core–shell catalyst, Pd@UiO-66-NH_2@mSiO_2, with Pd@UiO-66-NH_2 as the core and mesoporous SiO_2 (mSiO_2) as the shell. Scanning electron microscopy (SEM), X-ray diffraction (XRD) and Fourier transform infrared spectroscopy (FT-IR) measurement results demonstrated that the obtained catalyst has an excellent core–shell structure. It can significantly prevent the aggregation of Pd nanoparticles (NPs), as well as the leaching of Pd NPs during the reaction process, owing to the protective effect of mSiO_2. During the tandem reaction of aniline and benzaldehyde to generate secondary amines, the prepared Pd@UiO-66-NH_2@mSiO_2 is highly efficient, due to the strong acid sites provided by UiO-66-NH_2 and the hydrogenation reduction sites provided by Pd NPs. Meanwhile, the Pd@UiO-66-NH_2@mSiO_2 with porous structure can also enhance the mass transfer of reactants to improve the reaction efficiency. Additionally, the prepared catalyst was used to catalyze the series reaction of amino compounds and aldehydes, and the results showed that just 5 mg of the catalyst can convert more than 99% of the reactants within 60 minutes in the presence of 1 atm H_2 at room temperature. Finally, the selectivity and stability of the as-prepared catalyst were also confirmed.

Received 16th December 2022
Accepted 4th February 2023

DOI: 10.1039/d2ra08016h

rsc.li/rsc-advances

Introduction

Secondary amines are important intermediates in the synthesis of pharmaceuticals, cosmetics, fuels, and dyes.[1–6] The traditional methods for synthesizing secondary amines include reductive amination of carbonyl compounds,[7,8] direct nucleophilic substitution reactions between primary amines and alkylating reagents,[9] and organometallic additions between carbonyl compounds and highly reactive Grignard reagents or organic reagents.[10] However, the mentioned above methods for synthesizing secondary amines require relatively expensive raw materials, and the synthesis process is relatively complicated, which limits practical application to a large extent. The one-pot tandem reaction has attracted extensive attention in organic synthesis due to its characteristics of few synthesis steps, simple purification, high performance, less waste generated by atomic economy, and short reaction time.[11–13] And the one-pot tandem reaction of amino compounds with aldehydes provides an atom-economical and environmentally friendly method for the preparation of secondary amines.[14] The one-pot tandem process mainly involves two steps: firstly, the condensation of primary amines with aldehydes to form imines, followed by reductive hydrogenation of the imines to convert them to the corresponding secondary amines. In order to drive the tandem reaction, catalysts contain two kinds of sites, the solid acid sites are used to catalyze the condensation of primary amines and aldehydes, and the metal catalytic sites are utilized to catalyze the hydrogenation in required condition.[11,15] Catalysts with both sites are considered as promising alternatives for one-pot tandem reactions due to their relatively low corrosivity, high catalytic activity, high selectivity, and easy separation for subsequent use.[16] In recent years, scholars have favored multifunctional core–shell noble metal-based heterogeneous catalysts.[17–21] A noble metal is selected as an active site supported on a material that could not only act as catalyst site but also act as support as the catalyst core. And another material with high porosity and good stability is selected as the catalyst shell to design a core–shell catalyst for catalyzing the tandem reactions.[22,23]

It is critical to select the supports during the core–shell catalyst preparation procedure. It is proved that the combination of metal organic frameworks (MOFs) and noble metals has a broad prospect.[24–28] MOFs are a relatively new class of porous

[a]College of Chemical Engineering, Northwest Minzu University, Lanzhou, Gansu 730030, PR China. E-mail: lizhh02006@163.com; Fax: +86 931 4512932; Tel: +86 931 4512932

[b]State Key Laboratory of Applied Organic Chemistry, Laboratory of Special Function Materials and Structure Design of the Ministry of Education, College of Chemistry and Chemical Engineering, Lanzhou University, Lanzhou 730000, PR China. E-mail: dongzhp@lzu.edu.cn

† Electronic supplementary information (ESI) available. See DOI: https://doi.org/10.1039/d2ra08016h

materials that form open crystalline frameworks with permanent porosity by linking metal-containing units with organic linkers,[29–31] with tunable pore sizes, well-defined metal nodes, tunable chemical composition, and surface function.[32–36] There are many advantages to supporting the noble metals on the MOFs. For example: the noble metals NPs are highly dispersed on the MOFs to prevent NPs agglomeration and reduce metal load; the sites required for the catalysts can be obtained from the well-defined metal nodes; the tunable pore sizes may facilitate the ability to catalyze reactants with various molecular sizes.[37] Li *et al.*[38] reported MOF-derived core–shell catalysts Ni@NC for catalyzing one-pot reduction amination to prepare secondary amines exhibited excellent performance. In addition, Anderson *et al.*[39] successfully prepared a Pd-nanoparticle@MIL-101(Cr) catalyst for one-pot tandem reduction amination. However, there are still some challenges in designing core–shell catalysts when use MOFs as the supports. For instance, the metal NPs can easily leach from the supports and affect the catalytic performance and the metal nodes contained in the selected MOF cannot be used to catalyze the tandem reaction. In order to solve above problems, in this work, UiO-66-NH_2 was chosen as the support to carry noble metal NPs.[40] UiO-66-NH_2 introduced N source to anchor the metal NPs to prevent leaching during the reaction. Meanwhile, coordinatively unsaturated Zr site contained in UiO-66-NH_2 can catalyze the cascade reaction.[41,42]

Many studies on core–shell catalysts have confirmed that, anchoring noble metal NPs in the core,[43,44] and the existence of the shell ensures that the noble metal NPs can act alone in the microenvironment and protect the metal NPs from leaching and aggregation.[45,46] Adding noble metals into the core–shell catalysts is a key step in the catalytic cascade reaction. Zhang *et al.*[47] reported a stepwise self-assembly and concurrent self-etching strategy to prepare SiO_2@UiO-66-NH_2 hollow composite for Knoevenagel condensation (2-nitrobenzaldehyde and malononitrile). Due to the absence of noble metals, the catalytic reaction is relatively simple, which greatly limits the practical application. Additionally, shell is very important in the preparation of core–shell catalyst. Mesoporous silica ($mSiO_2$), which has high porosity and good stability, is often used as the shell of catalyst to improve the speed of mass transfer and catalyst activity in the reaction process.[48–50] Meanwhile, the coexisting $mSiO_2$ shell can protect the noble metal NPs from leaching and aggregation during the reaction.[51–53] In order to improve the stability of the catalyst and protect the leaching and aggregation of noble metal NPs, $mSiO_2$ was chosen as the shell to prepare the core–shell catalyst in this work.

Based on these, in this work, the noble metal Pd was supported on the UiO-66-NH_2 as the core and $mSiO_2$ was chosen as the shell, we successfully prepared Pd@UiO-66-NH_2@$mSiO_2$ core–shell catalyst with core–shell structure. The results showed that the prepared Pd@UiO-66-NH_2@$mSiO_2$ core–shell catalyst exhibited excellent catalytic performance in the reaction of amino compounds and aldehydes to secondary amines in the presence of hydrogen and at room temperature (25 °C, 1 atm H_2). Therefore, it provides a new route for designing multifunctional core–shell heterogeneous catalysts.

Experiment

Chemical materials

N,*N*-Dimethylformamide (DMF), 2-aminoterephthalic acid, zirconium tetrachloride ($ZrCl_4$), and acetic acid were purchased from Tianjin Haines Biochemical Technology Co., Ltd. Cetyltrimethylammonium bromide (CTAB), tetraethylorthosilicate (TEOS), palladium chloride ($PdCl_2$), ammonium nitrate (NH_4NO_3), and sodium borohydride ($NaBH_4$) were obtained by Tianjin Guangfu Fine Chemical Research Institute supply. Ethanol (EtOH), dimethyl sulfoxide (DMSO), tetrahydrofuran (THF) were purchased from Shanghai Alading Biochemical Technology Co., LTD. Amino compounds and aldehydes were obtained from Sinopharm Chemical Reagent Co., Ltd (China). Deionized water was made in laboratory. All chemicals were used without further purification.

Preparation of UiO-66-NH_2

UiO-66-NH_2 was prepared according to previously reported methods.[54,55] 0.48 g $ZrCl_4$ was dissolved in 120 mL DMF and sonicated for 5 minutes, then 0.372 g of 2-aminoterephthalic acid was added to the above solution, and continued to sonicate for 5 minutes. Then, 5.9 mL of acetic acid was added, and obtained solution was transferred to a Teflon-lined autoclave reactor and reacted at 120 °C for 24 h in an oven. The above solution was naturally cooled to room temperature and pink powder was collected by centrifugation, washed with ethanol for 3 times and activated in a vacuum oven at 80 °C for 24 h.

Preparation of Pd@UiO-66-NH_2

300 mg UiO-66-NH_2 was dispersed in 100 mL ethanol, 2.5 mL 6 mg mL^{-1} $PdCl_2$ aqueous solution was added dropwise, after stirring for 6 h, $NaBH_4$ solution was added for reduction, continued stirring for 6 h, finally black powder was collected by centrifugation and dried in a vacuum oven at 30 °C.

Preparation of Pd@UiO-66-NH_2@$mSiO_2$

375 g cetyltrimethylammonium bromide (CTAB), 300 mg Pd@UiO-66-NH_2 were dispersed in a mixed solution of 300 mL deionized water and 60 mL ethanol. After stirring at room temperature for 1 h, the temperature was increased to 50 °C, and then 1.5 mL $NH_3 \cdot H_2O$ was induced, finally the prepared solution (1880 μL tetraethylorthosilicate and 30 mL absolute ethanol) was added drop by drop in five times. The above solution was continuously stirred for 6 h and collected by centrifugation. The collected black powder was etched with 100 mL NH_4NO_3/ethanol solution (6 mg mL^{-1}) at 80 °C for 6 h, then collected by centrifugation, washed three times with ethanol and dried in a vacuum oven at 30 °C.

One-pot tandem synthesis of secondary amines

Typically, 1 mmol aniline, 0.5 mmol benzaldehyde and 5 mg Pd@UiO-66-NH_2@$mSiO_2$ catalyst were dispersed in a 10 mL round bottom flask with 3 mL solvent. The reaction system was then purged with H_2 ten times and stirred under a H_2

atmosphere at 25 °C for the indicated time. And the catalyst was collected by centrifugation after the reaction for subsequent use.

Recovery of catalyst

The reused catalyst before the eighth cycle was recovered for in a centrifuge at 12 000 RPM for 3 minutes, washed 3 times with anhydrous ethanol and dried in vacuum at 30 °C for 24 h.

Catalytic characterization

The morphological and structural characteristics of the as-prepared materials were analyzed by scanning electron microscopy (SEM, ThermoFisher Apero S) and transmission electron microscopy (TEM, FEI talos F200 s). The crystal structure of the catalysts were measured by powder X-ray diffraction (PXRD, Rigaku miniFlex 600), Powder X-ray diffraction (PXRD) patterns were recorded on a Rigaku miniFlex 600 with 2θ from 3–90. The functional groups in the catalysts were analyzed by Fourier-transform infrared spectroscopy (FT-IR, Bruker VERTEX 70). The valence states of different elements on the material surface were analyzed by X-ray photoelectron spectroscopy (XPS, PerkinElmer PHI-5702). The actual contents of metals in the catalyst were determined by inductively coupled plasma-optical emission spectroscopy (ICP-AES). The Brunauer–Emmett–Teller (BET, 3H-2000PSA2) method was used to analyze the specific surface area and pore size distribution. Nitrogen adsorption–desorption measurements were conducted at 77 K on a surface area and pore size analyzer (3H-2000PSA2) after the samples were degassed at 120 °C for 2 h. And selectivity measurement of one-pot cascade reactions was detected by gas chromatography (GC-2014 + AFSC, 230C) and gas chromatography-mass spectrometry (GC-MS, Agilent 5977E). Gas chromatogram and gas chromatogram-mass spectrometry were recorded by 230C and Agilent 5977E at 60–280 °C, respectively.

Results and analysis

As shown in Scheme 1, the preparation of Pd@UiO-66-NH_2@-$mSiO_2$ mainly included three steps. Firstly, the UiO-66-NH_2 metal organic framework was synthesized by using zirconium chloride and 2-aminoterephthalic acid as building blocks; secondly, the aqueous solution of palladium chloride was added dropwise into the ethanol solution of UiO-66-NH_2 by traditional dipping method, and then reduced with sodium borohydride to synthesize Pd@UiO-66-NH_2 as the core; The surface of Pd@UiO-66-NH_2 was subsequently covered by a $mSiO_2$ shell by the classical Stöber method.[56,57] CTAB was used as a mesoporous template and was removed by etching with NH_4NO_3/ethanol solution (6 mg mL^{-1}).

The structure changes of the materials during the preparation were detected by TEM. As shown in Fig. 1(a), the as-prepared UiO-66-NH_2 exhibits a hexahedral morphology. And Fig. 1(b) reveals that the Pd NPs of Pd@UiO-66-NH_2 uniformly dispersed on UiO-66-NH_2. As can be seen in Fig. 1(c) that after being coated with mesoporous SiO_2, the morphology of UiO-66-NH_2 remained unchanged, and the average particle size of Pd nanoparticles is 8–9 nm. According to the analysis of TEM images, the average size of Pd NPs in Pd@UiO-66-NH_2@$mSiO_2$ is almost unchanged compared with that in Pd@UiO-66-NH_2, indicating that the coating process of $mSiO_2$ and the effect of CTAB etching do not lead to aggregation of Pd NPs. In addition, the corresponding element mapping confirmed that Pd@UiO-66-NH_2@$mSiO_2$ contains N, O, Si, Zr, Pd and all these elements are uniformly distributed [Fig. 1(d)].

The XRD patterns of the three prepared materials are presented in Fig. 2(a). The diffraction pattern of UiO-66-NH_2 [curve 1 in Fig. 2(a)] is fitted with published standard simulation curves,[54,55,58] which illustrate the successful preparation of highly crystalline UiO-66-NH_2. There is no obvious crystallinity loss in Pd@UiO-66-NH_2 [curve 2 in Fig. 2(a)], demonstrating that the crystallinity of UiO-66-NH_2 does not affect by the addition of Pd NPs compared with UiO-66-NH_2. Interestingly, no diffraction peaks of Pd are observed, which may be due to the high dispersion and extremely small particle size of Pd NPs. Besides, there is a new broad peak that appeared around 20°, which corresponds to mesoporous SiO_2 (ref. 59) [curve 3 in Fig. 2(a)]. The loss of crystallinity after coating SiO_2 is due to the etching of SiO_2 with NH_4NO_3/ethanol solution to facilitate the formation of mesoporous structure. As illustrated in Fig. 2(b), the FT-IR spectrum of 2-aminoterephthalic acid is in good agreement with that reported literature.[60] The peak that centers that appear at 3505 cm^{-1} and 3388 cm^{-1} are attributed to the asymmetric stretching vibration of –NH_2 and the symmetric

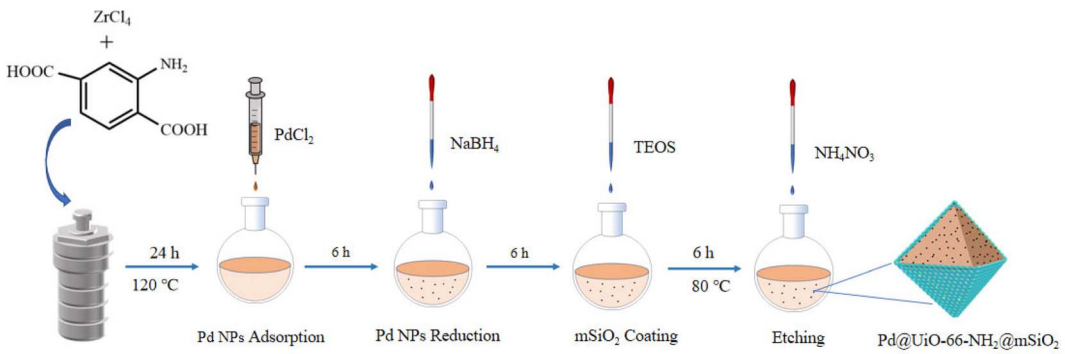

Scheme 1 The preparation process of Pd@UiO-66-NH_2@$mSiO_2$ catalyst.

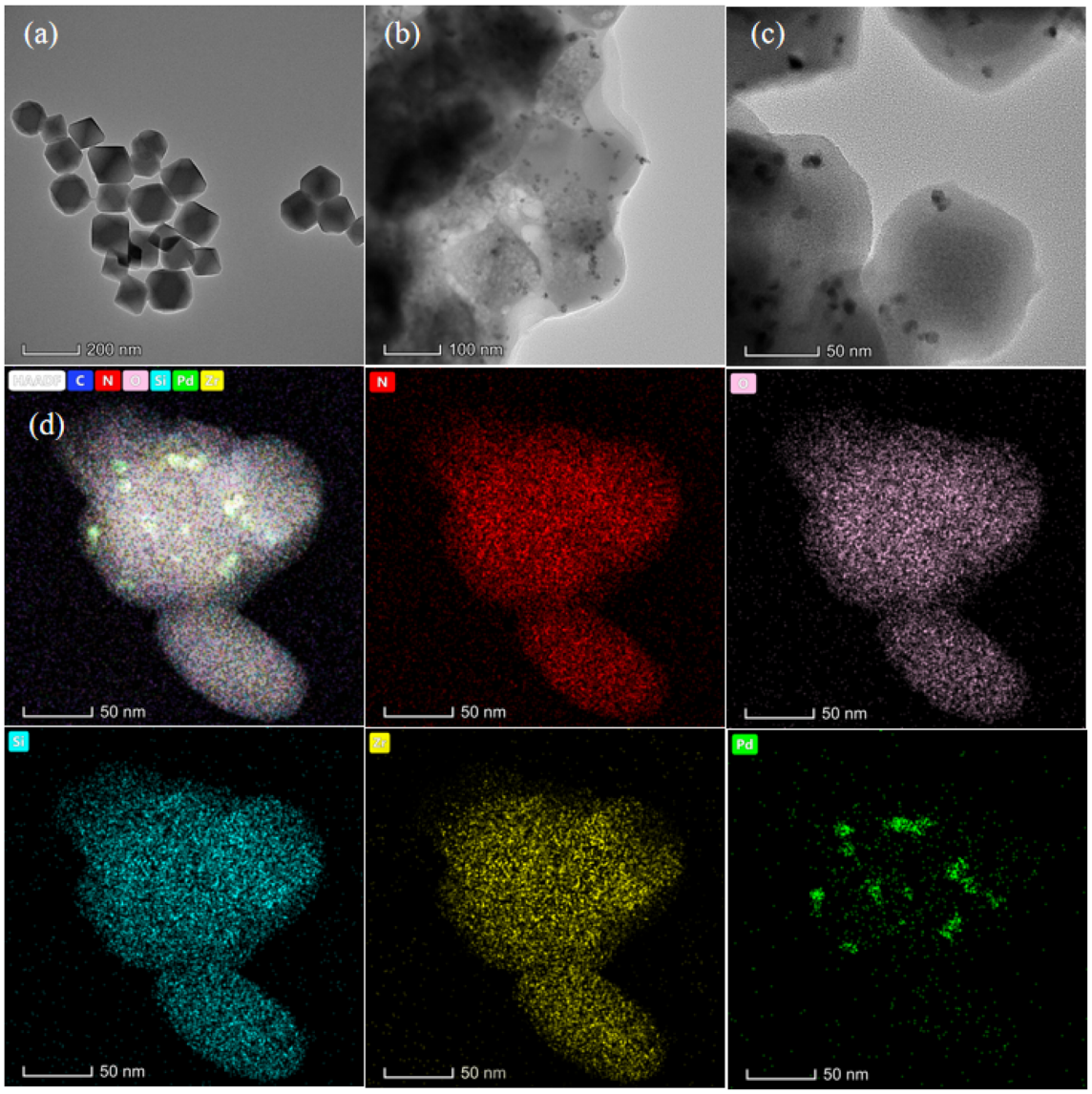

Fig. 1 TEM images of (a) UiO-66-NH_2, (b) Pd@UiO-66-NH_2, (c) Pd@UiO-66-NH_2@$mSiO_2$; (d) HAADF-STEM image of Pd@UiO-66-NH_2@$mSiO_2$ corresponding element mapping images for N, O, Si, Zr, and Pd.

stretching vibration of $-NH_2$, respectively. The weak peaks at 1661 cm^{-1} and 1660 cm^{-1} are ascribed to the bending vibration of N–H. The strong peaks at 1583 cm^{-1} and 1568 cm^{-1} are assigned to the C=O coupling of the symmetric stretching vibration with the ring vibration. And the peaks at 1219 cm^{-1} and 1158 cm^{-1} correspond to the stretching vibration of C–N on the aromatic ring. Furthermore, the peaks at the lower frequencies 661 cm^{-1} are attributed to the Zr–O modes,[59] which act as acidic sites in the catalyst.

As shown in Fig. 3, the elements contained in the prepared catalyst Pd@UiO-66-NH_2@$mSiO_2$ are C, N, O, Zr, Si, and Pd. Compared with UiO-66-NH_2, the peak intensities of N, Zr, and Pd in Pd@UiO-66-NH_2@$mSiO_2$ are weakened, because XPS can only detect the signal of elements with a certain sample thickness. The high-resolution C 1s spectrum exhibits two peaks at 284.6 eV, 285.6 eV which can be ascribed to C–C and C–O, respectively [Fig. 3(b)]. The high-resolution Zr 3d spectra of the two samples reveal two peaks at 182.9 eV and 185.2 eV, which are attributed to Zr $3d_{5/2}$ and Zr $3d_{3/2}$, respectively [Fig. 3(c)]. In addition, the Pd 3d peak in Pd@UiO-66-NH_2@$mSiO_2$ is deconvoluted into two peaks, Pd $3d_{5/2}$ and Pd $3d_{3/2}$ correspond to Pd^{2+} and Pd^0, respectively, and the coexisting Pd^{2+} may be due to the existence of Pd–N bonds [Fig. 3(d)]. It can be found on the XPS image that the peak intensity of Pd is very weak, possibly because Pd NPs are coated in $mSiO_2$ and only absorb part of the X-ray. Therefore, the actual loading of Pd was determined in Pd@UiO-66-NH_2@$mSiO_2$ to be 0.08 mmol% by ICP-OES as shown in Table S1.†

The specific surface area and pore size distribution of the synthesized materials are shown in Fig. 4 and Table S2.† As shown in Fig. 4(a), both UiO-66-NH_2 and Pd@UiO-66-NH_2 exhibit type I N_2 adsorption–desorption curves with specific

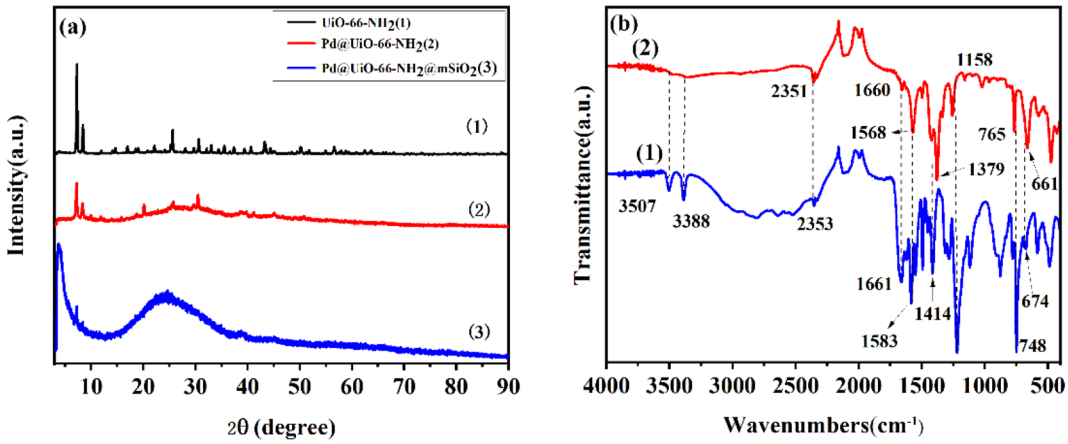

Fig. 2 (a) XRD patterns of (1) UiO-66-NH_2, (2) Pd@UiO-66-NH_2, (3) Pd@UiO-66-NH_2@$mSiO_2$; (b) FT-IR spectra of (1) 2-aminoterephthalic acid, (2) UiO-66-NH_2.

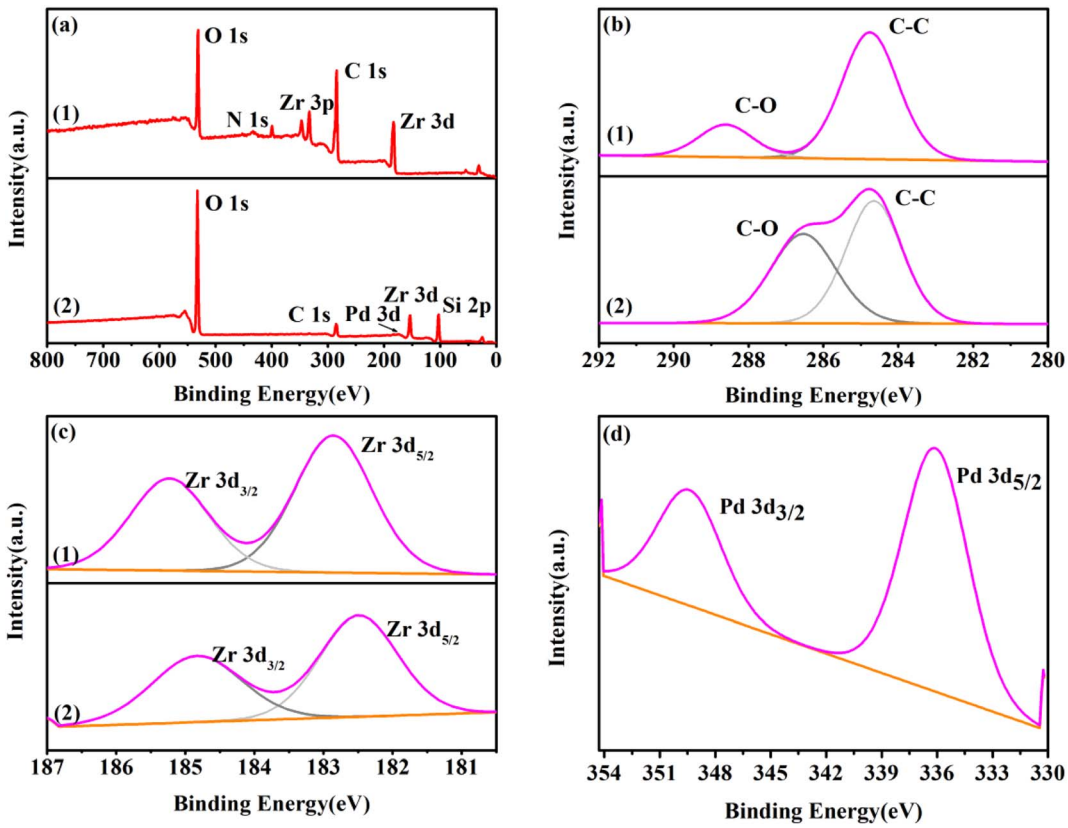

Fig. 3 (a) The wide-range XPS spectra; the high-resolution spectra of (b) C 1s, and (c) Zr 3d in (1) UiO-66-NH_2 and (2) Pd@UiO-66-NH_2@$mSiO_2$; (d) the high-resolution spectra of Pd in Pd@UiO-66-NH_2@$mSiO_2$.

surface areas of 1107.3 $m^2\ g^{-1}$ and 1002.6 $m^2\ g^{-1}$, respectively, demonstrating that the existence of mesoporous structures in the materials. With regard to UiO-Pd@UiO-66-NH_2@$mSiO_2$, a type I/IV N_2 adsorption–desorption isotherm exists and specific surface area is 920.3 $m^2\ g^{-1}$, indicating the simultaneous existence of microporous and mesoporous in this material because of the introduction of $mSiO_2$. Notably, the prepared materials with high specific surface area and pores can enhance the mass transfer of reactants during reaction.[61] The pore size distribution of the prepared materials is shown in Fig. 4(b), the pore size of Pd@UiO-66-NH_2@$mSiO_2$ is between 1.4–3.2 nm, and the size of Pd NPs is 8–9 nm, revealing that Pd NPs are in $mSiO_2$ and it is arduous to be leached from the pores under the encapsulation of $mSiO_2$.

In order to investigate the synergistic effect between the Pd sites and Lewis acid sites of the prepared Pd@UiO-66-

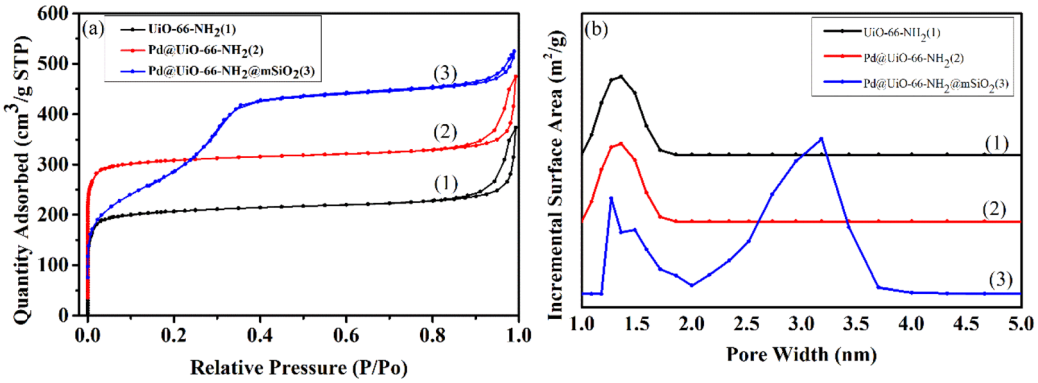

Fig. 4 (a) Nitrogen adsorption–desorption isotherms and (b) the corresponding pore sizes distribution curves of Pd@UiO-66-NH_2@$mSiO_2$.

NH_2@$mSiO_2$ catalyst, a one-pot cascade reaction of aniline and benzaldehyde was employed as a model reaction, and the reaction conditions were optimized with molecular hydrogen as the green hydrogen source under ambient pressure. At the same time, the results were compared with those reported in the previous literature.[62]

Firstly, this cascade reaction is not reacted without a catalyst (Table 1, entry 1). However, the conversion of this tandem reaction and the selectivity of the target product both reached more than 99% in the presence of Pd@UiO-66-NH_2@$mSiO_2$ catalyst (Table 1, entry 2). Meanwhile, the TOF under this condition is 618.75 h^{-1} and the TON is 618.75. The strong acid sites contained in UiO-66-NH_2 can promote the condensation of aniline and benzaldehyde to form imine.[63] Subsequently, the imine is hydrogenated to form *N*-benzylaniline under the action of the Pd metal sites. Then, the effect of solvents on the tandem reaction was also carried out. In comparison studies, ethanol was chosen as the solvent for this reaction to achieve the best conversion and highest selectivity (Table 1, entries 2, 5, 6, 7 and 8). At the same time, the reaction is also affected by the molar usage of the two initial reactants. When the molar amount of benzaldehyde used is more than or equal to the molar amount of aniline, benzaldehyde is preferentially converted to the side reactant benzyl alcohol, reducing the yield of the target product (Table 1, entry 9). Therefore, the use of excess aniline is the key to achieving high selectivity of the target product. To further investigate the catalytic properties of Pd@UiO-66-NH_2@$mSiO_2$, comparative experiments are also performed. When Pd@UiO-66-NH_2 (without $mSiO_2$ shell) is used as catalyst, due to the leaching of Pd active sites during the reaction, the selectivity of

Table 1 Optimizing the reaction conditions of catalytic one-pot reaction of aniline with benzaldehyde

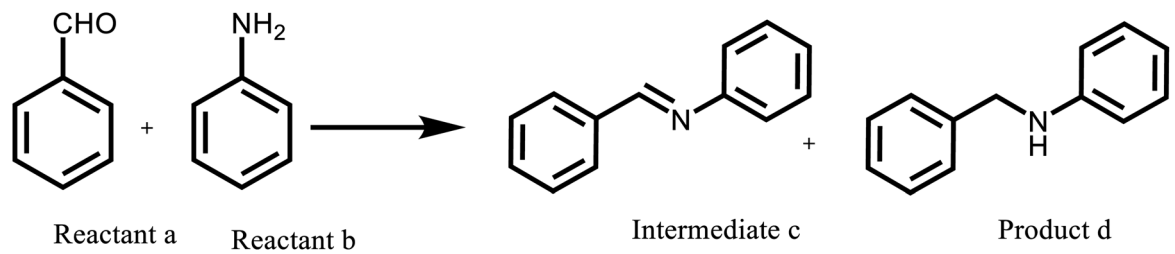

Entry	Catalyst	Solvent	Conv. (%)	c Sel. (%)	d Sel. (%)
1[a]	—	EtOH	—	—	—
2[a]	Pd@UiO-66-NH_2@$mSiO_2$	EtOH	>99	—	>99
3[a]	Pd@UiO-66-NH_2	EtOH	>99	58	42
4[a]	UiO-66-NH_2	EtOH	>99	>99	—
5[a]	Pd@UiO-66-NH_2@$mSiO_2$	DMSO	>99	96	4
6[a]	Pd@UiO-66-NH_2@$mSiO_2$	THF	>99	83	17
7[a]	Pd@UiO-66-NH_2@$mSiO_2$	H_2O	>99	72	28
8[a]	Pd@UiO-66-NH_2@$mSiO_2$	DMF	>99	50	50
9[b]	Pd@UiO-66-NH_2@$mSiO_2$	EtOH	>99	58	42
10[c]	SiNS–Pd	IPA	>99	—	>99

[a] Reaction conditions: 25 °C, atmospheric pressure, 5 mg catalyst, 0.5 mmol benzaldehyde, 1 mmol aniline, 3 mL solvent, H_2 balloon, reaction time: 1 h. [b] 1 mmol benzaldehyde. [c] 1 mmol aniline, 1.2 mmol benzaldehyde, 2 mL 2-propanol, 160 mg SiNS–Pd catalyst, 1.0 MPa H_2, 60 °C, reaction time: 18 h.[64]

Table 2 Optimizing the reaction conditions of catalytic one-pot reaction amines with aldehydes[a]

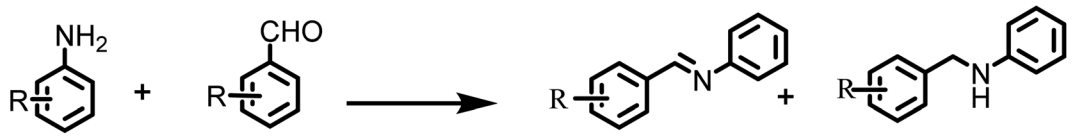

Reactant a Reactant b Intermediate c Product d

Entry	Substrate	Conv. (%)	c Sel. (%)	d Sel. (%)
1	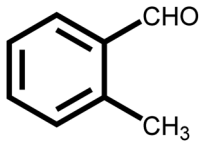	>99	—	>99
2	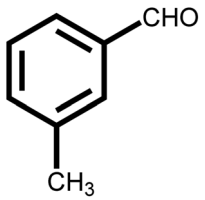	>99	—	>99
3	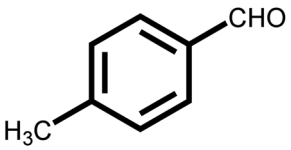	>99	—	>99
4	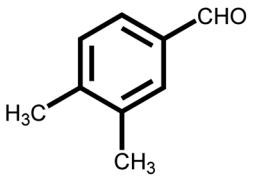	>99	4	96
5	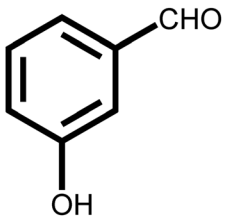	>99	—	>99
6	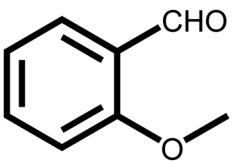	>99	—	>99
7	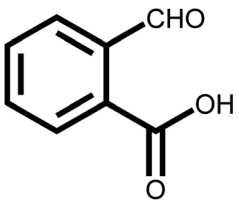	>99	—	>99

Table 2 (*Contd.*)

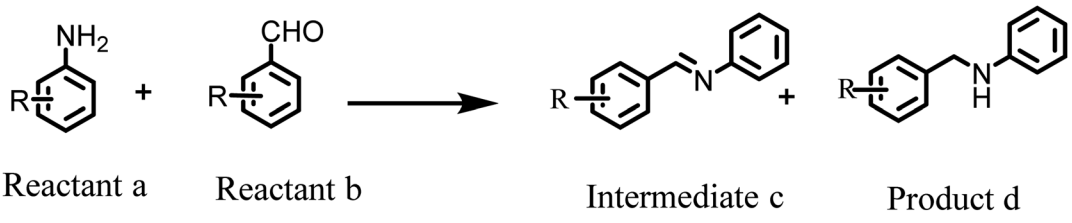

Reactant a Reactant b Intermediate c Product d

Entry	Substrate	Conv. (%)	c Sel. (%)	d Sel. (%)
8	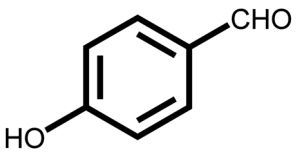	>99	—	>99
9	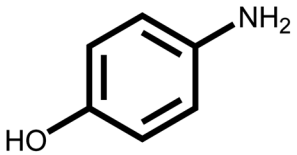	>99	—	>99
10	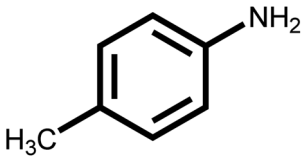	>99	—	>99
11	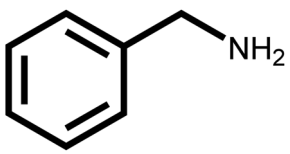	>99	—	>99

[a] Reaction conditions: 25 °C, atmospheric pressure, 5 mg catalyst, 0.5 mmol aldehydes, 1 mmol amines, 3 mL EtOH, H_2 balloon, reaction time: 1 h.

N-benzylaniline was significantly reduced, demonstrating that the protection of the $mSiO_2$ shell is a crucial factor for achieving excellent selectivity (Table 1, entry 3). As expected, the initial reactants could not be converted to the target product in this tandem reaction with UiO-66-NH_2, illustrating the critical role of the Pd sites in the reaction (Table 1, entry 4). Furthermore, compared with other catalyst (Table 1, entry 10), it is found that the initial reactant can be converted into the target product only under relatively harsh conditions (60 °C, 18 h, 160 mg catalyst).[64] In summary, the prepared catalyst enables the reaction of aniline and benzaldehyde to generate the target product under very mild conditions.

To further understand the general applicability of the Pd@UiO-66-NH_2@$mSiO_2$ core–shell catalyst, various amines as well as aldehydes were tested as reactants under the optimal reaction conditions.

As shown in Table 2, the initial reactants are converted into corresponding target products with high conversion and selectivity. There are excellent conversion rates and selectivity in 2-methylbenzaldehyde, 3-methylbenzaldehyde, and 4-methylbenzaldehyde, 3-hydroxybenzaldehyde, *o*-anisaldehyde, 2-carboxybenzaldehyde, *p*-hydroxybenzaldehyde, indicating the benzaldehydes containing only one functional group, the conversion and selectivity of the tandem reaction are not affected by the steric position of the group (Table 2, entries 1, 2, 3, 5, 6, 7 and 8). Meanwhile, the conversion and selectivity of aniline with only one functional group and benzylamine also perform well (Table 2, entries 9, 10 and 11). However, the selectivity is relatively low (96%) for 3, 4-dimethylbenzaldehyde containing two functional groups (Table 2, entry 4) to react with aniline into the target product may be attributed to steric hindrance. In addition, both reactants with electron-donating groups and electron-absorbing groups do not effect on the reaction, indicating that the influence of electronic effects is not obvious. In conclusion, the above results indicate that the efficient and selective one-pot synthesis of secondary amines using Pd@UiO-66-NH_2@$mSiO_2$ modified with different functional groups of amines and aldehydes under very mild conditions.

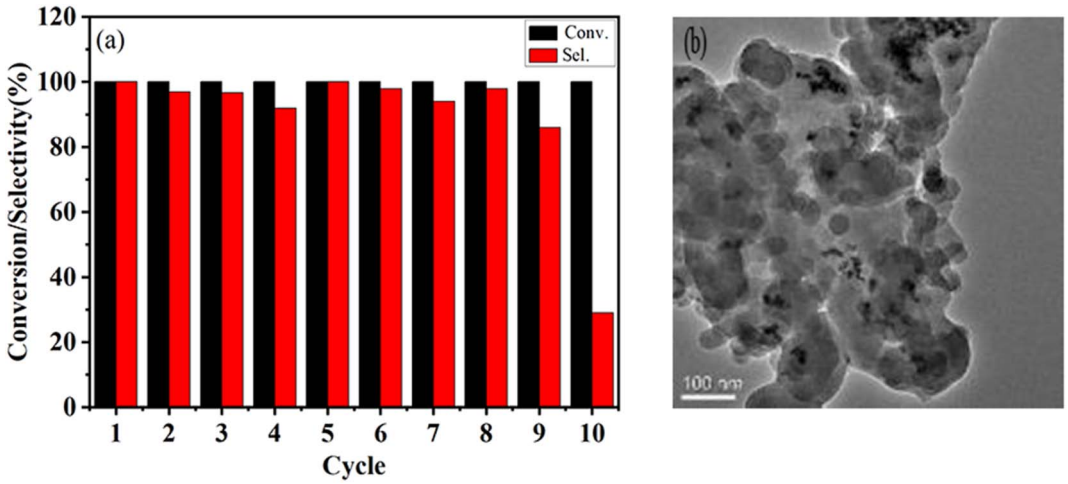

Fig. 5 (a) The recyclability of Pd@UiO-66-NH_2@$mSiO_2$ in the one-pot cascade reaction of benzaldehyde with aniline to corresponding secondary amines and (b) TEM image of Pd@UiO-66-NH_2@$mSiO_2$ after the eighth cycle.

To further understand the reaction process, the reaction time course and the as well as the target product distribution were carefully monitored (Fig. S1†).

It can be seen in Fig. S1† that benzaldehyde and aniline can be completely converted into imine intermediate within 10 minutes under the function of the acidic sites of Pd@UiO-66-NH_2@$mSiO_2$. Subsequently, the imine intermediate is reduced by H_2 with the extension of time with the assistance of the Pd sites, and the target product *N*-benzylaniline is rapidly formed.

Besides, the stability of the Pd@UiO-66-NH_2@$mSiO_2$ core–shell catalyst under the optimum reaction conditions is also investigated. As shown in Fig. 5(a), Pd@UiO-66-NH_2@$mSiO_2$ exhibits excellent catalytic performance. The high activity is maintained even after 9 cycles, and a selectivity of 84% to the corresponding secondary amine is obtained, due to the protective effect of $mSiO_2$, so that the Pd NPs were not leached during the catalytic reaction (Table 1, entry 2). The selectivity of the tenth cycle dropped sharply to 23%, possibly due to the aggregation of Pd NPs during the recovery process [Fig. 5(b)]. These results indicate that the core–shell structure of UiO-66-NH_2@Pt@$mSiO_2$ can effectively maintain the stability of the catalyst.

Conclusions

In this study, a dual-site core–shell catalyst UiO-66-NH_2@-Pt@$mSiO_2$ was prepared. The as-prepared catalyst exhibited excellent catalytic activity and stability for the one-pot cascade conversion of amino compounds and aldehydes to secondary amines under mild conditions (25 °C, 1 atm H_2), due to the fact that UiO-66-NH_2 provided acid sites for condensation of initial reactants, and Pd NPs provided hydrogenation sites for further hydrogenation of imine intermediates. Additionally, the new prepared catalyst could be recycled up at least 8 times proving that Pd NPs are protected by $mSiO_2$ and will not be leached during the reaction. In summary, the reasonable design of Pd@UiO-66-NH_2@$mSiO_2$ catalyst in this work provides an approach for the preparation of other multifunctional catalysts in the future.

Conflicts of interest

The authors declare no conflicts of interest.

Acknowledgements

This work is supported by the National Natural Science Foundation of China (No. 31760608), Fundamental Research Fund for the Central Universities, Northwest Minzu University (No. 31920210069 and 31920200002), the Key Program of Natural Science Foundation of Gansu Province (No. 22JR5RA178), the Key Talent Projects in Gansu Province and the Natural Science Foundation of Gansu Province (No. 21JR1RA198) and the Lanzhou Chengguan District Science and Technology Plan Project (2022JSCX0009).

References

1 O. I. Afanasyev, E. Kuchuk, D. L. Usanov and D. Chusov, *Chem. Rev.*, 2019, **119**, 11587–11911.
2 C. Chen, R. Fan, M. Han, X. Zhu, Y. Zhang, H. Zhang, H. Zhao and G. Wang, *Appl. Catal., B*, 2021, **280**, 119448.
3 X. Wang, B. Zhu, J. Dong, H. Tian, Y. Liu, H. Song and Q. Wang, *Chem. Commun.*, 2021, **57**, 5028–5031.
4 H.-O. Kim, B. Carroll and M. S. Lee, *Synth. Commun.*, 1997, **27**, 2505–2515.
5 A. Singh, S. M. Mobin and P. Mathur, *Dalton Trans.*, 2018, **47**, 14033–14040.
6 A. Takeshima, T. Kano and K. Maruoka, *Org. Lett.*, 2019, **21**, 8071–8074.
7 Y. Kita, S. Kai, L. B. Supriadi Rustad, K. Kamata and M. Hara, *RSC Adv.*, 2020, **10**, 32296–32300.
8 F. A.-M. Ahmed and J. M. Steven, *Org. Process Res. Dev.*, 2006, **10**, 971–1031.

9 S. L. Montgomery, J. Mangas-Sanchez, M. P. Thompson, G. A. Aleku, B. Dominguez and N. J. Turner, *Angew. Chem., Int. Ed.*, 2017, **56**, 10491–10494.
10 M. Hatano, S. Suzuki and K. Ishihara, *J. Am. Chem. Soc.*, 2006, **128**, 9998–9999.
11 C. Chen, N. Janoszka, C. K. Wong, C. Gramse, R. Weberskirch and A. H. Gröschel, *Angew. Chem., Int. Ed.*, 2020, **60**, 237–241.
12 J. A. T. Caetano and A. C. Fernandes, *Green Chem.*, 2018, **20**, 2494–2498.
13 X. Chen, S. Han, D. Yin and C. Liang, *Inorg. Chem. Front.*, 2020, **7**, 82–90.
14 Y. Zhang, Y. Gao, S. Yao, S. Li, H. Asakura, K. Teramura, H. Wang and D. Ma, *ACS Catal.*, 2019, **9**, 7967–7975.
15 K. S. Nagi Reddy, K. P. Reddy and G. Sabitha, *ChemistrySelect*, 2018, **3**, 13670–13674.
16 R. Javad Kalbasi and S. F. Rezayi, *J. Porous Mater.*, 2018, **26**, 641–654.
17 Y. Huang, B. Wang, H. Yuan, Y. Sun, D. Yang, X. Cui and F. Shi, *Catal. Sci. Technol.*, 2021, **11**, 1652–1664.
18 F. Meemken and A. Baiker, *Chem. Rev.*, 2017, **117**, 11522–11569.
19 T. G. Ulusoy Ghobadi, E. Akhuseyin Yildiz, M. Buyuktemiz, S. Sadigh Akbari, D. Topkaya, Ü. İsci, Y. Dede, H. G. Yaglioglu and F. Karadas, *Angew. Chem., Int. Ed.*, 2018, **57**, 17173–17178.
20 F. F. Tao, W. T. Ralston, H. Liu and G. A. Somorjai, *J. Phys. Chem. B*, 2017, **122**, 425–431.
21 H. C. Lima dos Santos, M. A. Gonçalves, A. da Cas Viegas, B. A. Miranda Figueira, P. T. Souza da Luz, G. Narciso da Rocha Filho and L. R. Vieira da Conceição, *RSC Adv.*, 2022, **12**, 34614–34626.
22 S. Dai, K. P. Ngoc, L. Grimaud, S. Zhang, A. Tissot and C. Serre, *J. Mater. Chem. A*, 2022, **10**, 3201–3205.
23 B. Zhang and Y. Qin, *ACS Catal.*, 2018, **8**, 10064–10081.
24 W. Xu, K. B. Thapa, Q. Ju, Z. Fang and W. Huang, *Coord. Chem. Rev.*, 2017, **373**, 199–232.
25 M. Zhong, S. Zhang, A. Dong, Z. Sui, L. Feng and Q. Chen, *J. Mater. Sci.*, 2020, **55**, 10388–10398.
26 A. Saeed, X.-Y. Zhang, Z.-Q. Huang, X.-Y. Zhao, L. Xu, Y. Zhao, W.-Y. Sun and J. Zhao, *RSC Adv.*, 2022, **12**, 35461–35468.
27 C. Liu, K. Quan, H. Li, X. Shi, J. Chen and H. Qiu, *Chem. Commun.*, 2022, **58**, 13111–13114.
28 F. G. Cirujano, I. Luz, M. Soukri, C. Van Goethem, I. F. J. Vankelecom, M. Lail and D. E. De Vos, *Angew. Chem., Int. Ed.*, 2017, **56**, 13302–13306.
29 J. Dong, X. Han, Y. Liu, H. Li and Y. Cui, *Angew. Chem., Int. Ed.*, 2020, **59**, 13722–13733.
30 M. A. Alnaqbi, A. Alzamly, S. H. Ahmed, M. Bakiro, J. Kegere and H. L. Nguyen, *J. Mater. Chem. A*, 2021, **9**, 3828–3854.
31 M. Xie, J. Wang, X.-L. Du, N. Gao, T. Liu, Z. Li, G. Xiao, T. Li and J.-Q. Wang, *RSC Adv.*, 2022, **12**, 32518–32525.
32 X. Fang, Q. Shang, Y. Wang, L. Jiao, T. Yao, Y. Li, Q. Zhang, Y. Luo and H.-L. Jiang, *Adv. Mater.*, 2018, **30**, 1705112.
33 C.-C. Hou, H.-F. Wang, C. Li and Q. Xu, *Energy Environ. Sci.*, 2020, **13**, 1658–1693.
34 L. Jiao and H.-L. Jiang, *Chem*, 2019, **5**, 786–804.
35 X. Shi, Y. Lin, L. Huang, Z. Sun, Y. Yang, X. Zhou, E. Vovk, X. Liu, X. Huang, M. Sun, S. Wei and J. Lu, *ACS Catal.*, 2020, **10**, 3495–3504.
36 S. Ko, F. Gao, X. Yao, H. h. Yi, X. Tang, C. Wang, H. Liu, N. Luo and Z. Qi, *New J. Chem.*, 2022, **46**, 15758–15775.
37 M. Liu, J. Wu and H. Hou, *Chem.–Eur. J.*, 2018, **25**, 2935–2948.
38 J. Li, B. Wang, Y. Qin, Q. Tao and L. Chen, *Catal. Sci. Technol.*, 2019, **9**, 3726–3734.
39 A. E. Anderson, C. J. Baddeley and P. A. Wright, *Catal. Lett.*, 2017, **148**, 154–163.
40 X. Chen, Y. Lyu, Z. Wang, X. Qiao, B. C. Gates and D. Yang, *ACS Catal.*, 2020, **10**, 2906–2914.
41 X. Fan, F. Xin, W. Zhang and H. Liu, *React. Funct. Polym.*, 2022, **17**, 105260.
42 Y. Xu, L. Chen, Y. Zhang, Y. Huang, J. Cao and W. Jiang, *Food Chem.*, 2022, **404**, 134427.
43 Y. Long, S. Song, J. Li, L. Wu, Q. Wang, Y. Liu, R. Jin and H. Zhang, *ACS Catal.*, 2018, **8**, 8506–8512.
44 S. Zhang, A. Han, Y. Zhai, J. Zhang, W.-C. Cheong, D. Wang and Y. Li, *Chem. Commun.*, 2017, **53**, 9490–9493.
45 F. Fu, C. Wang, Q. Wang, A. M. Martinez-Villacorta, A. Escobar, H. Chong, X. Wang, S. Moya, L. Salmon, E. Fouquet, J. Ruiz and D. Astruc, *J. Am. Chem. Soc.*, 2018, **140**, 10034–10042.
46 Y. Yun, H. Sheng, K. Bao, L. Xu, Y. Zhang, D. Astruc and M. Zhu, *J. Am. Chem. Soc.*, 2020, **142**, 4126–4130.
47 Y. Zhang, X. Zhang, T. Dai and J. Li, *Mater. Lett.*, 2019, **240**, 44–46.
48 A. Pramanik and S. Bhar, *New J. Chem.*, 2021, **45**, 16355–16388.
49 N. An, Y. Wang, M. Li, H. Lin and F. Qu, *New J. Chem.*, 2018, **42**, 18318–18327.
50 W. Li, Y. Tian, B. Zhang, L. Tian, X. Li, H. Zhang, N. Ali and Q. Zhang, *New J. Chem.*, 2015, **39**, 2767–2777.
51 R. Zanella, A. Sandoval, P. Santiago, V. A. Basiuk and J. M. Saniger, *J. Phys. Chem. B*, 2006, **110**, 8559–8565.
52 K. Wang, K. Zhao, Q. Meng, Q. Bai, X. Li, H. Hu, H. Jiao and Y. Tang, *RSC Adv.*, 2022, **12**, 35452–35460.
53 M. Zare and L. Moradi, *RSC Adv.*, 2022, **12**, 34822–34830.
54 Z. Guo, C. Xiao, R. V. Maligal-Ganesh, L. Zhou, T. W. Goh, X. Li, D. Tesfagaber, A. Thiel and W. Huang, *ACS Catal.*, 2014, **4**, 1340–1348.
55 J. H. Cavka, S. Jakobsen, U. Olsbye, N. Guillou, C. Lamberti, S. Bordiga and K. P. Lillerud, *J. Am. Chem. Soc.*, 2008, **130**, 13850–13851.
56 A. F. Demirörs, A. van Blaaderen and A. Imhof, *Chem. Mater.*, 2009, **21**, 979–984.
57 S. Bao, J. Li, B. Guan, M. Jia, O. Terasaki and J. Yu, *Matter*, 2020, **3**, 498–508.
58 X. Li, Z. Guo, C. Xiao, T. W. Goh, D. Tesfagaber and W. Huang, *ACS Catal.*, 2014, **4**, 3490–3497.
59 H. Zhao, B. Li, H. Zhao, J. Li, J. Kou, H. Zhu, B. Liu, Z. Li, X. Sun and Z. Dong, *J. Colloid Interface Sci.*, 2021, **606**, 1524–1533.

60 J. Heiska, M. Nisula, E.-L. Rautama, A. J. Karttunen and M. Karppinen, *Dalton Trans.*, 2020, **49**, 1591–1599.
61 D. Yue, J. Lei, L. Zhou, X. Du, Z. Guo and J. Li, *Arabian J. Chem.*, 2020, **13**, 2649–2658.
62 Y. Hoshimoto, T. Kinoshita, S. Hazra, M. Ohashi and S. Ogoshi, *J. Am. Chem. Soc.*, 2018, **140**, 7292–7300.
63 K. Mishra, S. H. Kim and Y. R. Lee, *ChemSusChem*, 2019, **12**, 881–889.
64 T. Sato, Y. Uozumi and Y. M. A. Yamada, *ACS Omega*, 2020, **5**, 26938–26945.